J Braz. Soc. Mech. Sci. Eng. (2016) 38:433–441
DOI 10.1007/s40430-015-0342-4

TECHNICAL PAPER

A central compact scheme for numerical solution of two-phase incompressible flow using Allen–Cahn phase field model

Muhammad Rizwan[1,2] · **Abdullah Shah**[1] · **Li Yuan**[2]

Received: 21 November 2014 / Accepted: 16 March 2015 / Published online: 31 March 2015

Abstract This article presents a numerical method for the Allen–Cahn phase field model coupled with the incompressible Navier–Stokes equations for simulating two-phase incompressible flow. The numerical method is based on the artificial compressibility method with dual-time stepping technique applied to the governing equations written in conservative form. The convective terms are approximated by using an eighth-order central compact scheme with filtering while the viscous terms are approximated by a sixth-order central compact scheme. Approximate factorization-based alternating direction implicit algorithm is used to solve the discretized linear system. The effectiveness of the method is demonstrated by computing several benchmark two-phase incompressible flow problems.

Keywords Two-phase flow · Phase field model · Artificial compressibility · Dual-time stepping · Central compact scheme

Technical Editor: Fernando Alves Rochinha.

✉ Muhammad Rizwan
rizwanbsm@gmail.com

Abdullah Shah
scholar.cm@gmail.com

Li Yuan
lyuan@lsec.cc.ac.cn

[1] Department of Mathematics, COMSATS Institute of Information Technology, Park Road Chak Shahzad, Islamabad, Pakistan

[2] Institute of Computational Mathematics and Scientific/Engineering Computing, Academy of Mathematics and Systems Science, Chinese Academy of Sciences, Beijing 100190, China

1 Introduction

The nature of the interface between two fluids has been the subject of extensive investigations in scientific and engineering applications. However, there are several causes of difficulty in formulating accurate solution models even for the simplest set of systems. For example, physical properties like interfacial tension make multi-fluid flows difficult to treat analytically and numerically. In an immiscible two-fluid system, the components are separated by a sharp interface that evolves in time with the fluid flow. From the mathematical point of view, this problem is called moving boundary or free surface problem. There are two types of models to formulate the interfacial flow problems, the sharp interface and the diffusive interface models.

The initial investigations on free surface problems by Young, Laplace and Gauss [1] considered the sharp interface endowed with some physical properties such as surface tension between two fluids. Many surface properties such as capillarity, are associated with the surface tension through special boundary conditions on the interfaces [2–5]. In classical sharp interface approaches like front-tracking method [6], boundary integral method [7], level set method [8], and coupled level set/VOF method [9], the physical properties are discontinuous across the interface and are described by some physical boundary conditions and the interface usually evolves in time. The drawback of this approach is the need to explicitly track the dynamic interface at each time step. On the other hand, in the (diffusive interface) phase field models [10, 11], the sharp fluid interface is replaced by a thin but nonzero thickness transitional layer where the interfacial forces are smoothly distributed. One does not need to track the moving interface explicitly at each time step. The most appealing feature of the phase field model is its ability to

deal with distinct problems (immiscible or miscible) by a single set of equations, therefore, phase field models are becoming popular choices for modeling multi-phase flows and a wide range of phase transition problems in material sciences.

In a previous study [12], we found that numerical discretization and coding of the phase field model were simple in the framework of the artificial compressibility method (ACM) [13], in the belief that time (pseudo-time) marching of a hyperbolic system may be easier than mixed time marching and solving of an elliptic system with large gradients at interfaces. The time accuracy of the ACM for unsteady flows was no longer a big problem with the advent of dual-time stepping technique [14, 15]. We have used WENO scheme together with the ACM in [12], but found that although WENO scheme was very robust to calculate flows with thin interface layer, it incurred excessive numerical diffusion near the interface layer. A high-order accurate, high-resolution central compact finite difference scheme with suitable filtering [16, 17] is expected to better resolve the thin diffusive layer, especially for cases where there are massive vortex flows developed from the interfaces. In the present paper we apply an eighth-order central compact finite difference scheme with tenth-order filtering as proposed in [16, 17] for solving the Allen–Cahn phase field model [11, 18].

The rest of the paper is organized as follows. The governing equations for the mixture of two incompressible fluids are given in Sect. 2. In Sect. 3, the artificial compressibility formulation is written in conservative form. Section 4 explains the spatial discretization. Time discretization and approximate factorization-based alternating direction implicit (AF-ADI) algorithm are given in Sect. 5. Numerical tests in several two-dimensional problems on the mixture of two incompressible fluids are given in Sect. 6 and finally conclusions are given in Sect. 7.

2 Phase field model for mixture of two incompressible fluids

Let Ω be a two-dimensional physical domain with the Cartesian coordinate system. We further assume that Ω is filled with two incompressible viscous fluids separated by a free moving interface. The phase-field function $\phi(\mathbf{x},t)$ assumes distinct constant values in each bulk phase and undergoes rapid but smooth variation in the interfacial region. The phase-field is used to identify the two fluids and the interface at any time t. For simplicity, we only consider a specific type of mixture of two incompressible fluids with same density ($\rho = 1$) and same viscosity constants [11]. We have the following system of equations:

$$\nabla\cdot\mathbf{u} = 0, \tag{1a}$$

$$\mathbf{u}_t + (\mathbf{u}\cdot\nabla)\mathbf{u} - \mu\Delta\mathbf{u} + \nabla p = \mathbf{b} - \lambda\Delta\phi\nabla\phi, \tag{1b}$$

$$\phi_t + (\mathbf{u}\cdot\nabla)\phi - \gamma\Delta\phi = \gamma(-f(\phi) + \xi(t)), \tag{1c}$$

$$\frac{\mathrm{d}}{\mathrm{d}t}\int_\Omega \phi \mathrm{d}\mathbf{x} = 0. \tag{1d}$$

The coupled nonlinear system (1) will be subject to the initial conditions

$$\mathbf{u}|_{t=0} = \mathbf{u}_0, \quad \phi|_{t=0} = \phi_0$$

and appropriate boundary conditions. $\mathbf{u}$ is the fluid velocity, $p = p + \frac{1}{2}|\nabla\phi|^2$ is the redefined pressure [20] and constant μ is the viscosity, λ is the surface tension coefficient, γ the elastic relaxation time of the two-fluid system and $f(\phi)$ is a given polynomial function [11]. The buoyancy force $\mathbf{b}$ with gravitational acceleration g in the negative y direction is given as

$$\mathbf{b} = (0, -g(\rho - \rho_0))^T = \left(0, -\frac{1}{2}g(1+\phi)(\rho_1 - \rho_0) - \frac{1}{2}g(1-\phi)(\rho_2 - \rho_0)\right)^T$$

with $\rho = \frac{1+\phi}{2}\rho_1 + \frac{1-\phi}{2}\rho_2$, where ρ_1 and ρ_2 are the densities of fluid 1 and fluid 2, respectively, if $\phi = 1$ then $\rho = \rho_1$ and if $\phi = -1$ then $\rho = \rho_2$. The role of the Lagrange multiplier $\xi(t)$ in the Allen–Cahn Eq. (1c) is to change the asymptotic constant values (± 1) of the phase function ϕ so as to conserve the volume fraction. The original $\xi(t)$ is modified as $\xi(t)\left(1-\phi^2\right)$ because this will keep the maximum principle for ϕ as noted in [19]. The new $\xi(t)$ can be calculated by using the following formula got from (1d)

$$\xi(t) = \int_\Omega f(\phi)\mathrm{d}\mathbf{x} \Big/ \int_\Omega \left(1-\phi^2\right)\mathrm{d}\mathbf{x}.$$

3 Artificial compressibility formulation

By adding the artificial compressibility terms with dual-time stepping technique, and using the function f given in [11] and new $\xi(t)$, the system (1) in two space dimensions can be rewritten as follows:

$$\begin{aligned}
&p_\tau + \beta(u_x + v_y) = 0,\\
&u_\tau + u_t + \left(u^2 + p\right)_x + (uv)_y - \mu(u_{xx} + u_{yy}) = b_x - \lambda\phi_x(\phi_{xx} + \phi_{yy}),\\
&v_\tau + v_t + (uv)_x + \left(v^2 + p\right)_y - \mu(v_{xx} + v_{yy}) = b_y - \lambda\phi_y(\phi_{xx} + \phi_{yy}),\\
&\phi_\tau + \phi_t + (u\phi)_x + (v\phi)_y - \gamma(\phi_{xx} + \phi_{yy}) = \gamma\left(1-\phi^2\right)\left(\frac{\phi}{\eta^2} + \xi(t)\right).
\end{aligned} \tag{2}$$

Write the above equations in conservative form:

$$\mathbf{Q}_\tau + \mathbf{I}_m\mathbf{Q}_t + (\mathbf{E} - \mathbf{E}_v)_x + (\mathbf{F} - \mathbf{F}_v)_y = \mathbf{S}_{\mathrm{int}}, \tag{3}$$

with

$$\mathbf{Q}=\begin{bmatrix} p \\ u \\ v \\ \phi \end{bmatrix},\quad \mathbf{E}=\begin{bmatrix} \beta u \\ u^2+p \\ uv \\ u\phi \end{bmatrix},\quad \mathbf{F}=\begin{bmatrix} \beta v \\ uv \\ v^2+p \\ v\phi \end{bmatrix},$$

$$\mathbf{I}_m=\begin{bmatrix} 0 & 0 & 0 & 0 \\ 0 & 1 & 0 & 0 \\ 0 & 0 & 1 & 0 \\ 0 & 0 & 0 & 1 \end{bmatrix},\quad \mathbf{E}_v=\begin{bmatrix} 0 \\ \mu u_x \\ \mu v_x \\ \gamma \phi_x \end{bmatrix}\quad \mathbf{F}_v=\begin{bmatrix} 0 \\ \mu u_y \\ \mu v_y \\ \gamma \phi_y \end{bmatrix},$$

and

$$\mathbf{S}_{\text{int}}=\begin{bmatrix} 0 \\ b_x-\lambda\phi_x\left(\phi_{xx}+\phi_{yy}\right) \\ b_y-\lambda\phi_y\left(\phi_{xx}+\phi_{yy}\right) \\ \gamma\left(1-\phi^2\right)\left(\phi/\eta^2+\xi(t)\right) \end{bmatrix}.$$

Here $\mathbf{Q}$ is the solution vector, u and v are Cartesian velocity components, p is the redefined pressure [20], ϕ is the phase variable of the species, constant η represents the diffusive interface width, β is the artificial compressibility parameter, τ is the pseudo-time and t is the physical time. The matrix $\mathbf{I}_m$ is a modified identity matrix. Subscripts τ, t, x, y represent partial derivatives. Because of the addition of the artificial compressibility terms, Eq. (3) become hyperbolic with respect to the pseudo-time, evidenced from all real eigenvalues of the Jacobian matrices $\mathbf{A}=\partial\mathbf{E}/\partial\mathbf{Q}$ and $\mathbf{B}=\partial\mathbf{F}/\partial\mathbf{Q}$ of the inviscid flux vectors. The viscous Jacobian matrices $\mathbf{A}_v$ and $\mathbf{B}_v$ of the viscous flux vectors, which will be utilized in the approximate factorization scheme, are

$$\mathbf{A}_v=\frac{\partial\mathbf{E}_v}{\partial\mathbf{Q}}=\text{diag}(0,\mu,\mu,\gamma)\partial_x,\quad \mathbf{B}_v=\frac{\partial\mathbf{F}_v}{\partial\mathbf{Q}}=\text{diag}(0,\mu,\mu,\gamma)\partial_y. \tag{4}$$

It is possible to diagonalize $\mathbf{A}$ and $\mathbf{B}$ as

$$\mathbf{A}=\mathbf{X}\Lambda_A\mathbf{X}^{-1},\quad \mathbf{B}=\mathbf{Y}\Lambda_\mathbf{B}\mathbf{Y}^{-1}, \tag{5}$$

where diagonal matrices Λ_A and Λ_B contain the eigenvalues of matrices $\mathbf{A}$ and $\mathbf{B}$:

$$\text{diag}\Lambda_A=\{u,u+c_1,u-c_1,u\},\quad \text{diag}\Lambda_B=\{v,v+c_2,v-c_2,v\}, \tag{6}$$

with $c_1=\sqrt{u^2+\beta}$ and $c_2=\sqrt{v^2+\beta}$ being the pseudo-speeds of sound. The matrices $\mathbf{X}$ and $\mathbf{Y}$ are the right eigenvectors matrices, while $\mathbf{X}^{-1}$ and $\mathbf{Y}^{-1}$ are their inverses, respectively. The detail is given in [12].

4 Spatial discretization: central compact scheme and filtering scheme

The eighth-order implicit central compact scheme in tri-diagonal form proposed by [21], is used to approximate the convective terms in Eq. (3) which can be expressed as

$$\alpha E'_{i-1}+E'_i+\alpha E'_{i+1}=a\frac{E_{i+1}-E_{i-1}}{2\Delta x}+b\frac{E_{i+2}-E_{i-2}}{4\Delta x}+c\frac{E_{i+3}-E_{i-3}}{6\Delta x}. \tag{7}$$

The values of the coefficients a, b, c and α in Eq. (7) for different order of the schemes are given in [21]. For the eighth-order scheme, the values are $a=\frac{25}{16}$, $b=\frac{1}{5}$, $c=-\frac{1}{80}$ and $\alpha=\frac{3}{8}$.

For the domain consisting of N points, the eighth-order compact scheme is applied directly to the interior points but for a non-periodic boundary, we used one-sided higher-order biased schemes of Zhang and Qian [22] to retain the original tri-diagonal form because adequate boundary closure is required for a non-periodic boundary for highly efficient computations. If the order of the boundary scheme is only one order lower than the interior points, the global formal accuracy will generally not degrade [23] and the stability of the computation can also be retained. Therefore, in the present numerical tests we used the seventh and sixth-order formulas near to boundary points. The seventh-order accuracy is expected and a tri-diagonal form is retained. Since the central compact schemes are non-dissipative and susceptible to numerical instabilities, high-order numerical filtering procedure is needed to control the instabilities originated from mesh non-uniformities, nonlinear flow features and boundary conditions. Spectral-type filters are applied as a post-processing stage after each time step integration to each component p, u, v and ϕ of the solution vector $\mathbf{Q}$ separately. If the unfiltered component of solution vector is denoted by ψ and the filtered component by $\hat{\psi}$ then tenth-order implicit filtering scheme [16] is of the form

$$\alpha_f\hat{\psi}_{i-1}+\hat{\psi}_i+\alpha_f\hat{\psi}_{i+1}=\sum_{m=0}^{M}\frac{a_m}{2}(\psi_{i+m}+\psi_{i-m}) \tag{8}$$

For multi-dimensional problems, the filter is applied sequentially in each of the three directions. Equation (8) provides a $2M$th-order formula on a $2M+1$ point stencil. The $M+1$ coefficients, $a_0, a_1, a_2, \ldots, a_{M-1}, a_M$ are derived in terms of the free parameter α_f. The parameter α_f which is in the range $-0.5<\alpha_f<0.5$, determines the filtering properties. High values of the parameter α_f yield less dissipative filters. Special treatments are required at points near the boundary because of the relatively large stencil of the filter. In this paper, The higher-order one-side biased formulas introduced in [17] are used to retain the accuracy of the scheme. Details of the filtering schemes can be found in [16], in which the values at the end boundary points are not filtered and can be given directly by physical or artificial boundary conditions, as suggested by those authors. The relatively large stencil of high-order filters

requires special formulations at several points near the boundaries. For instance, the tenth-order ($M = 5$) interior filter require 11-points stencil and thus cannot be applied at the near-boundary points $1, \ldots, 5$ and corresponding at $i\max - 4, \ldots, i\max$, so the following formulas retain the tri-diagonal form of the scheme,

$$\alpha_f \hat{\psi}_{i-1} + \hat{\psi}_i + \alpha_f \hat{\psi}_{i+1} = \sum_{m=1}^{11} a_{m,i}\psi_m, \quad (2 \le i \le 5),$$
$$\alpha_f \hat{\Psi}_{i-1} + \hat{\Psi}_i + \alpha_f \hat{\psi}_{i+1} = \sum_{m=0}^{10} a_{m,i}\psi_m, \quad (i\max - 4 \le i \le i\max - 1).$$

The values at points $i = 1$ and $i\max$ are specified explicitly through the boundary conditions and are not filtered. The extensive list of the coefficients for the higher-order, one-side filters at the left and right boundary is given in [16].

5 Implicit approximate factorization scheme

The approximate factorization (AF) method [24] is an extension of the alternating direction implicit (ADI) method to the system of the Euler and Navier–Stokes equations. Applying backward difference to the pseudo-time derivative and three-point, second-order backward difference to the physical-time derivative, we obtain

$$\frac{\Delta\mathbf{Q}^{n+1,m}}{\Delta\tau} + \mathbf{I}_m \frac{1.5\mathbf{Q}^{n+1,m+1} - 2\mathbf{Q}^n + 0.5\mathbf{Q}^{n-1}}{\Delta t} + \left[\frac{\partial(\mathbf{E} - \mathbf{E}_v)}{\partial x} + \frac{\partial(\mathbf{F} - \mathbf{F}_v)}{\partial y}\right]^{n+1,m+1} = \mathbf{S}_{\text{int}}^{n+1,m} \tag{9}$$

where $\Delta\mathbf{Q}^{n+1,m} = \mathbf{Q}^{n+1,m+1} - \mathbf{Q}^{n+1,m}$, the superscript n is the physical-time level and m is the pseudo-time level (the number of sub-iterations). $\Delta\tau$ is the pseudo-time step size which is determined based on the CFL number and Δt is the physical-time step size determined according to temporal resolution and trial. The equations are iterated in pseudo-time so that $\mathbf{Q}^{n+1,m+1}$ approaches the physical $\mathbf{Q}^{n+1}$ when the iteration is converged. The residual terms at $m + 1$ pseudo-time level are linearized with respect to the previous level m by using first-order Taylor's expansion, e.g.,

$$\mathbf{E}^{m+1} \approx \mathbf{E}^m + \left(\frac{\partial \mathbf{E}}{\partial \mathbf{Q}}\right)^m (\mathbf{Q}^{m+1} - \mathbf{Q}^m) = \mathbf{E}^m + \mathbf{A}^m \Delta\mathbf{Q}^m. \tag{10}$$

From now on, the superscript $n + 1$ is omitted for brevity. One can obtain the unfactored implicit delta form from Eq. (9) as

$$\left[\mathbf{I} + 1.5\frac{\Delta\tau}{\Delta t}\mathbf{I}_m + \Delta\tau\left(\frac{\partial(\mathbf{A} - \mathbf{A}_v)}{\partial x} + \frac{\partial(\mathbf{B} - \mathbf{B}_v)}{\partial y}\right)\right]^m \Delta\mathbf{Q}^m = -\Delta\tau\left(\frac{\partial(\mathbf{E} - \mathbf{E}_v)}{\partial x} + \frac{\partial(\mathbf{F} - \mathbf{F}_v)}{\partial y} - \mathbf{S}_{\text{int}}\right)^m - \frac{\Delta\tau}{\Delta t}\mathbf{I}_m\left(1.5\mathbf{Q}^m - 2\mathbf{Q}^n + 0.5\mathbf{Q}^{n-1}\right) = \mathbf{S}^m, \tag{11}$$

The terms $\mathbf{A}_v$ and $\mathbf{B}_v$ are the viscous Jacobian matrices in Eq. (4). The Beam–Warming approximate factorization scheme [24] can be symbolically written as

$$\pounds \cdot \Delta\mathbf{Q}^m \approx \pounds_x \pounds_y \cdot \Delta\mathbf{Q}^m = \mathbf{S}^m. \tag{12}$$

To obtain block tri-diagonal equations, convective terms in LHS of Eq. (11) are discretized by first-order upwind difference and viscous terms by conventional second-order central difference, e.g.,

$$\delta_x^+ f_i = \frac{f_{i+1} - f_i}{\Delta x}, \quad \delta_x^- f_i = \frac{f_i - f_{i-1}}{\Delta x}, \quad \text{and}$$
$$\delta_x^2 f_i = \frac{(f_{i+1} - 2f_i + f_{i-1})}{\Delta x^2}.$$

Remember that high-order central compact scheme is still used for the convective terms and a sixth-order central compact difference scheme [21] for the second derivative in the viscous and capillary terms in the RHS. After discretization of the LHS, one obtains the following form

$$\left[\mathbf{I} + 1.5\frac{\Delta\tau}{\Delta t}\mathbf{I}_m + \Delta\tau\left(\delta_x^-\mathbf{A}^+ + \delta_x^+\mathbf{A}^- - \delta_x\mathbf{A}_v\right) + \Delta\tau\left(\delta_y^-\mathbf{B}^+ + \delta_y^+\mathbf{B}^- - \delta_y\mathbf{B}_v\right)\right]^m \Delta\mathbf{Q}^m = \mathbf{S}^m. \tag{13}$$

In order to make use of the diagonal algorithm which saves computational cost [25, 26], we change $\mathbf{I}_m$ to $\mathbf{I}$ and $\text{diag}(0, \mu, \mu, \gamma)$ to $\max(\mu, \gamma)\mathbf{I}$ in the LHS of Eq. (13), which alters convergence rate but not accuracy. Denote $\left(1 + 1.5\frac{\Delta\tau}{\Delta t}\right)\mathbf{I} = \mathbf{H}$, then the equation becomes

$$\left[\mathbf{H} + \Delta\tau\left(\delta_x^-\mathbf{X}\Lambda_A^+\mathbf{X}^{-1} + \delta_x^+\mathbf{X}\Lambda_A^-\mathbf{X}^{-1} - \mu\mathbf{I}\delta_x^2\right) + \Delta\tau\left(\delta_y^-\mathbf{Y}\Lambda_B^+\mathbf{Y}^{-1} + \delta_y^+\mathbf{Y}\Lambda_B^-\mathbf{Y}^{-1} - \mu\mathbf{I}\delta_y^2\right)\right]^m \Delta\mathbf{Q}^m = \mathbf{S}^m.$$

As tradition, by adding cross-derivative terms to LHS, which is the same order of $\Delta\tau^3$ as the truncated terms of original equations, we can obtain the AF scheme according to x and y directions in the following form

$$\left[\mathbf{H} + \Delta\tau\left(\delta_x^- X\Lambda_A^+\mathbf{X}^{-1} + \delta_x^+ X\Lambda_A^-\mathbf{X}^{-1} - \mu\mathbf{I}\delta_x^2\right)\right]\mathbf{H}^{-1} \times \left[\mathbf{H} + \Delta\tau\left(\delta_y^- Y\Lambda_B^+\mathbf{Y}^{-1} + \delta_y^+ Y\Lambda_B^-\mathbf{Y}^{-1} - \mu\mathbf{I}\delta_y^2\right)\right]\Delta\mathbf{Q}^m = \mathbf{S}^m. \tag{14}$$

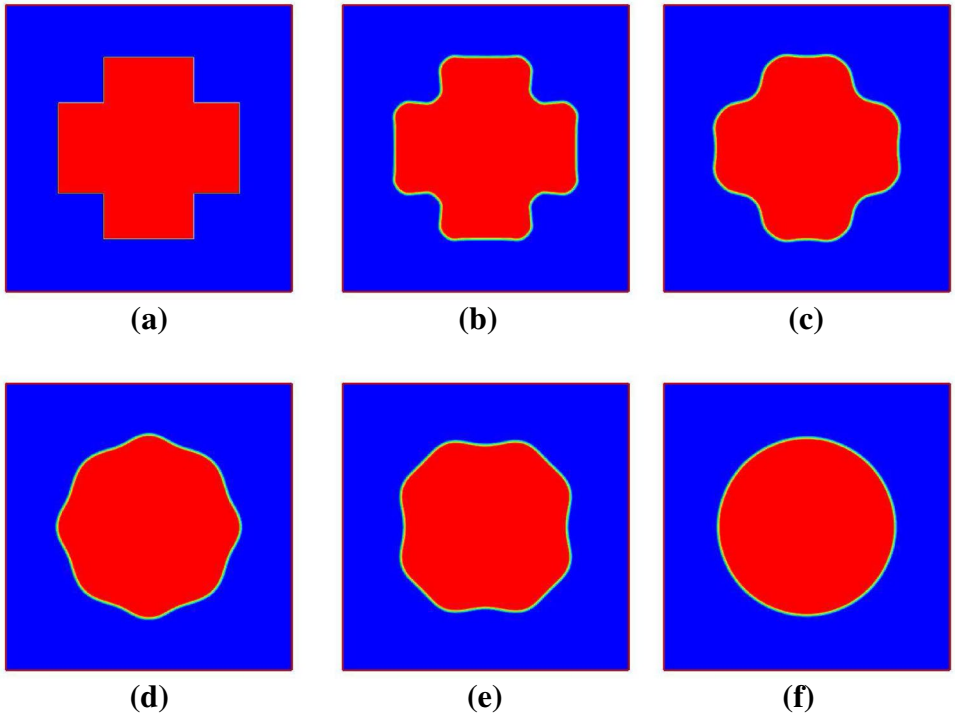

Fig. 1 Contours of ϕ for the cross to circle problem at different times with Lagrange multiplier. **a** $t = 0.0$, **b** $t = 0.04$, **c** $t = 0.1$, **d** $t = 0.4$, **e** $t = 0.6$, **f** $t = 19.8$

The system (14) can be solved with the well-known ADI scheme. In each direction, we need to solve a system of scalar tri-diagonal equations like

$$\alpha_i \Delta U_{i-1} + \beta_i \Delta U_i + \gamma_i \Delta U_{i+1} = r_i, \quad i = 2, \ldots, i\,\max - 1$$

with appropriate boundary conditions. In order to keep numerical stability, the split eigenvalues in the LHS of Eq. (14) are constructed as $\Lambda^{\pm} = \frac{1}{2}(\Lambda \pm \kappa|\Lambda|)$, where κ is a constant that is greater than or equal to unity to ensure

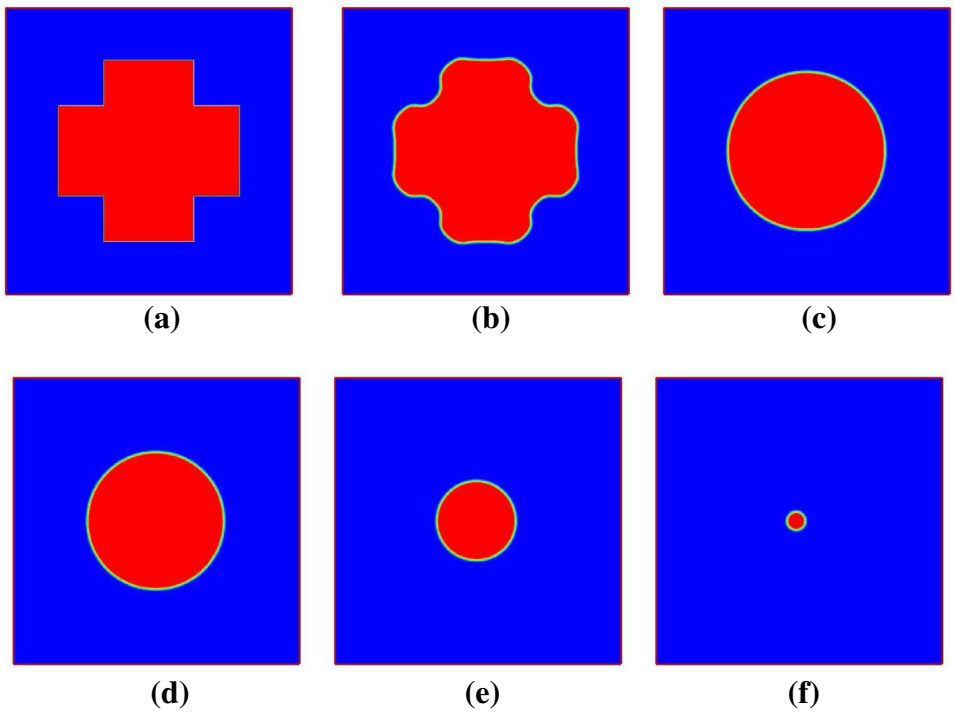

Fig. 2 Contours of ϕ for the cross to circle problem at different times without Lagrange multiplier. **a** $t = 0.0$, **b** $t = 0.08$, **c** $t = 4.0$, **d** $t = 8.0$, **e** $t = 16.0$, **f** $t = 19.8$

the split eigenvalue is strictly positive or negative. $\kappa = 1$ is used throughout this work.

6 Numerical examples

In this section, the numerical method developed in previous sections is tested against several 2D problems of incompressible two-fluid mixture with the same density as well as slightly different fluid density (the latter is treated with Boussinesq approximation as in [11]). In all computations, we have used following fixed physical parameters

$$\eta = 0.02, \quad \lambda = 0.1, \quad \mu = 0.1, \quad \text{and} \quad \gamma = 0.1$$

and the computational grid is 321×321 uniform grid points for a square solution domain $[0, 2\pi] \times [0, 2\pi]$. Time step Δt is set to 0.002 to be comparable to that used in references [11, 19, 27]. The maximum number of subiterations is set to 100. The initial velocity and pressure are all zero, while the initial condition for ϕ is specified in each example. We remark that the mesh size $2\pi/320 = 0.0196$ is comparable to the interfacial width $\eta = 0.02$, implying that the diffusive layer is under-resolved.

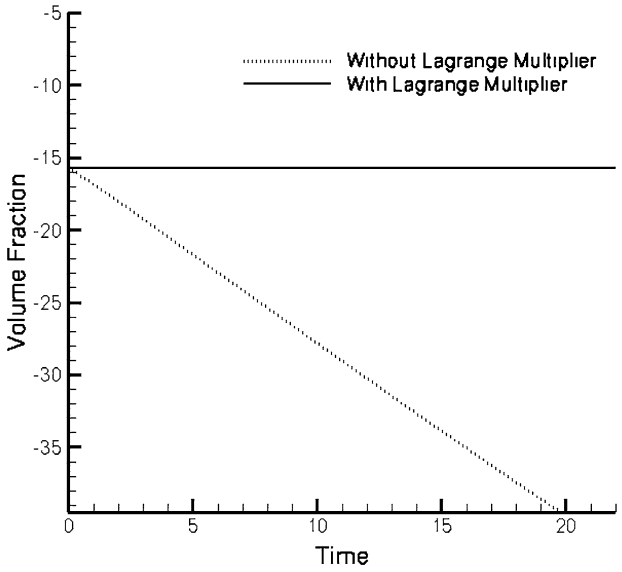

Fig. 3 Total volume fraction ($\int_\Omega \phi dx$) versus time to show mass conservation

6.1 Surface tension effect: cross to circle

In this example, initially a cross is centered at $[x, y] = [\pi, \pi]$. ϕ is taken 1 inside the cross and -1 otherwise as shown in Fig. 1. The computational domain $[0, 2\pi] \times [0, 2\pi]$ is partitioned with uniform mesh size. The cross initially with sharp corners is finally deformed into a circle. This evolution of phase exhibits the fact that the Allen–Cahn equation handles the sharp corners and minimizes the size of the interface. The final state of deformation is a steady state circle with a minimum size of the interface. The results in Fig. 1 shows that the cross deforms into circle because of surface tension effect. However, if we remove the Lagrange multiplier from the phase field equation, the cross will start

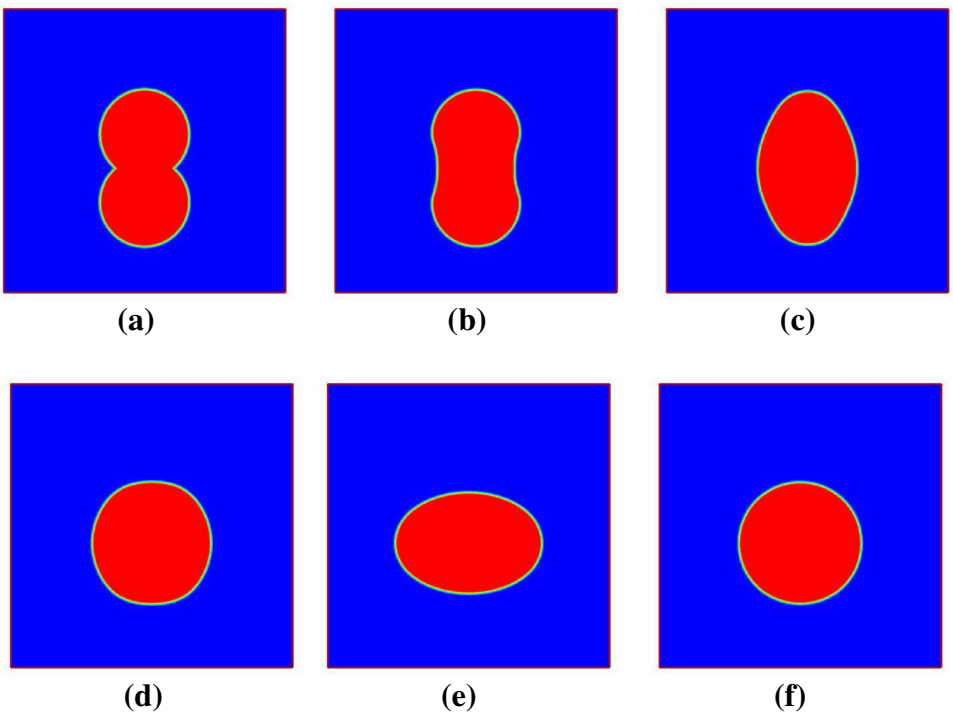

Fig. 4 Evolution of phase contours of coalescence of two bubbles at different times. **a** $t = 0.0$, **b** $t = 0.1$, **c** $t = 0.4$, **d** $t = 0.8$, **e** $t = 1.6$, **f** $t = 4.0$

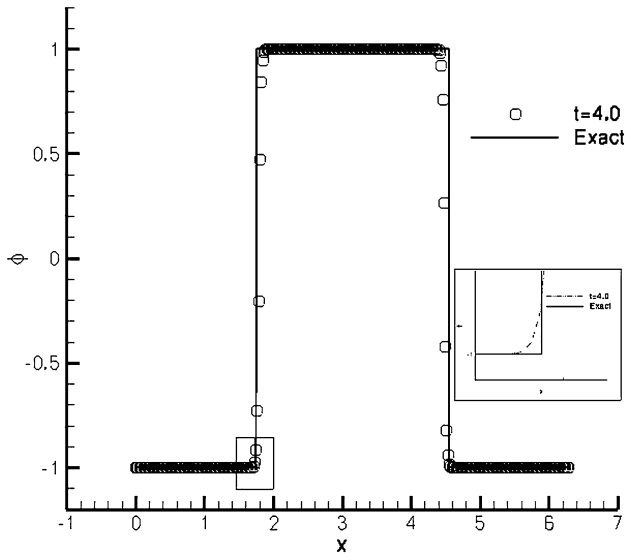

Fig. 5 The phase ϕ along $y = 3.0$. The *symbol circle* represents numerical solution and *solid line* represent exact value at $t = 4.0$

shrinking as shown in Fig. 2. With Lagrange multiplier, the volume of the bubble is preserved while it decreases gradually without Lagrange multiplier, as shown in Fig. 3. The results obtained with the present central scheme are in good agreement with those obtained with the finite element method [28].

6.2 Coalescence of two bubbles

This example is to study coalescence of two kissing bubbles due to surface tension and is simulated at different times. The computational domain is $[0, 2\pi] \times [0, 2\pi]$ with uniform mesh size. Initially, two unit circular bubbles are centered at $[\pi, 3.5]$ and $[\pi, 2]$ with radius 1, respectively. As the time evolves, first the two bubbles coalesce into one big and an elliptical bubble, which then transfigure and deforms into a circular bubble Fig. 4. This is the combination of the surface tension effect and the elastic effect from the phase equation. The results shown in Fig. 4 are well comparable with the results of Bao et al. [29]. The

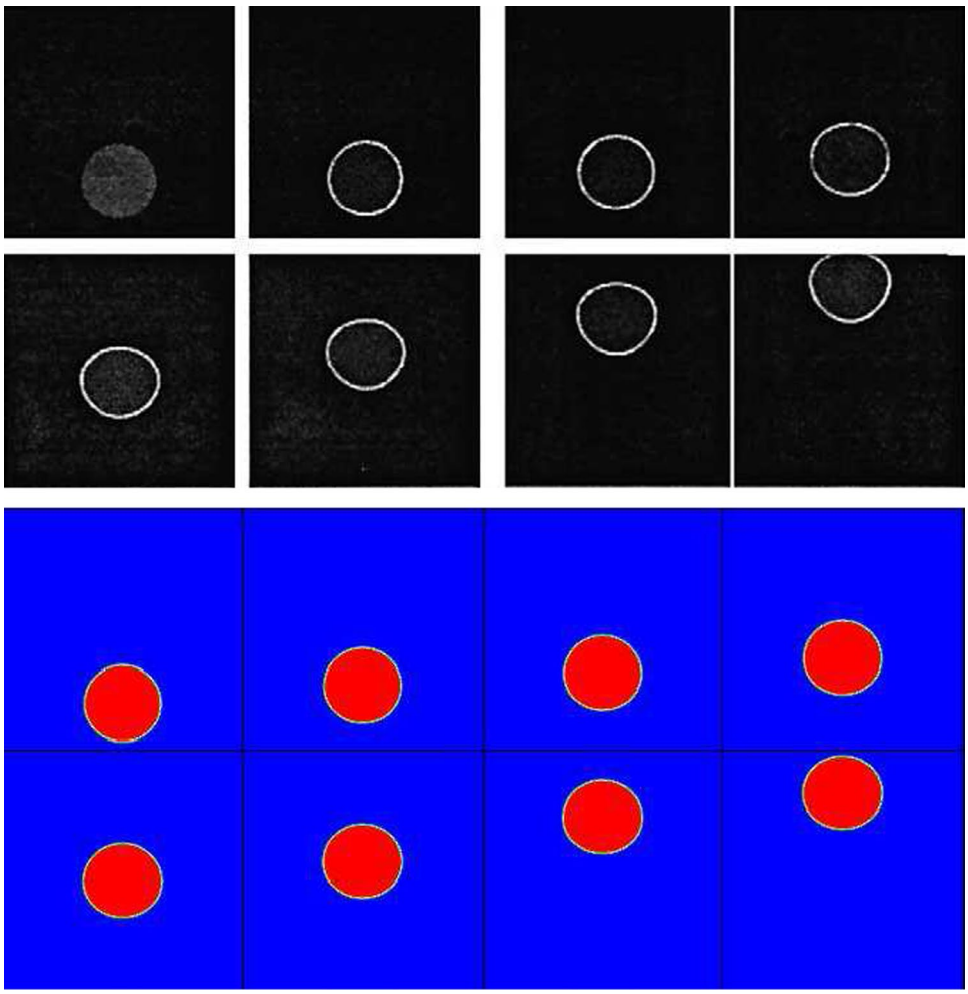

Fig. 6 Comparison of evolution of phase contours for $\rho_1 - \rho_2 = -0.1, g = 10$ at $t = 0.0, 1.5, 2.0, 2.5, 3.0, 3.5, 4.5, 5.0$

Table 1 Preservation of norm for example 3

Grid size	Error $= \|\phi(\mathbf{x}, t) - \phi_{\text{Exact}}\|_2$
129×129	1.14×10^{-2}
257×257	2.59×10^{-3}
321×321	5.49×10^{-5}

distribution of computed ϕ along $y = 3.0$ is shown in Fig. 5 for $t = 4.0$ having smooth values at the sharp corners (shown by zooming the left corner) and comparable with exact values of ϕ.

6.3 Rising bubbles

In this example, slightly different densities inside and outside of a bubble is considered. Boussinesq approximation as used in [11, 12] is adopted here. This example of rising bubble consists of a circular bubble of radius $r = 1$ centered at $(x_0, y_0) = (\pi, 1.2)$ in a domain of $[0, 2\pi] \times [0, 2\pi]$ with solid boundary walls using grid size 321×321. The density of the bubble is smaller than that of the surrounding fluid. The evolution of the bubbles are tracked for different times with Reynolds number $Re = 10(\mu = 0.1)$ while the density difference is $\rho_1 - \rho_2 = -0.1$ and $g = 10$. The results are shown in Fig. 6 which are well comparable with the results of [11]. We have also checked the preservation of the magnitude of the phase field function ϕ everywhere. It is expected to satisfy $\|\phi(\cdot, t)\| = 1$ because we have used the modified formula (1c) in which $\xi(t)$ is replaced by $\xi(t)(1 - \phi^2)$. Table 1 shows that the ϕ is satisfactorily kept at ± 1, when the grid refines, the error is $<10^{-4}$.

7 Conclusions

We have developed a numerical method using high-order central compact scheme for simulating incompressible two-phase flows. The governing equations are Allen–Cahn type phase field equation for the mixture of two incompressible fluids and the incompressible Navier–Stokes equations. The eighth-order central compact scheme with tenth-order filtering is successfully applied to the artificial compressibility formulation of the phase field model. The resulting linear system is solved with the approximate factorization-based alternating direction implicit (AF-ADI) algorithm. Several numerical examples have been used to show the effectiveness of the present method. The main attraction of the phase field model is its capability to easily incorporate the interface with smooth transition of physical quantities. However, the thickness of the interface is closely related to the range of molecular interactions, thus may be very different for various interface dynamics. In particular, cases with small thickness pose difficulty to numerical methods. In future work, we wish to resolve the thin width difficulty and go beyond of the Boussinesq approximation to solve more general multi-phase flow problems.

Acknowledgments This work was carried out while M. Rizwan and A. Shah were visiting ICMSEC, AMSS, Chinese Academy of Sciences under TWAS-CAS Postgraduate Fellowship and TWAS-UNESCO associateship scheme, respectively. M. Rizwan gratefully acknowledges Higher Education Commission (HEC) of Pakistan for the PhD fellowship. L. Yuan thanks the support of NSFC Grants (11261160486, 11321061) and 973 Project (2010CB731505).

References

1. Young T (1805) An essay on the cohesion of fluids. Philos Trans R Soc Lond 95:65–87
2. Chaikin PM, Lubensky TC (1995) Principles of condensed matter physics. Cambridge University Press, Cambridge
3. Edwards DA, Brenner H, Wasan DT (1991) Interfacial transport process and rheology. Butterworths/Heinemann, London
4. Krotov VV, Rusanov AI (1999) Physicochemical hydrodynamics of capillary systems. Imperial College Press, London
5. Probstein RF (1994) Physicochemical hydrodynamics: an introduction. Wiley, New York
6. Unverdi S, Tryggvason G (1992) A front-tracking method for viscous, incompressible, multifluid flows. J Comput Phys 100:25–37
7. Hou TY, Lowengrub JS, Shelley MJ (2001) Boundary integral methods for multicomponent fluids and multi-phase materials. J Comput Phys 169:302–362
8. Osher S, Sethian JA (1988) Fronts propagation with curvature-dependent speed: algorithm based on Hamilton–Jacobi formulations. J Comput Phys 79:12–49
9. Yang X, Lowengrub AJ, Zheng X, Cristini V (2006) An adaptive coupled level-set/volume-of-fluid interface capturing method for unstructured triangular grids. J Comput Phys 217:364–394
10. Anderson DM, McFadden GB, Wheeler AA (1998) Diffuse-interface methods in fluid mechanics. Appl Math Lett 30:139–165
11. Liu C, Shen J (2003) A phase-field model for the mixture of two incompressible fluids and its approximation by a Fourier-spectral method. Physica D 179:211–228
12. Shah A, Yuan L (2011) Numerical solution of a phase field model for incompressible two-phase flows based on artificial compressibility. Comput Fluids 42:54–61
13. Chorin AJ (1967) A numerical method for solving incompressible viscous flow problems. J Computat Phys 2:12–26
14. Rogers SE, Kwak D (1990) An upwind differencing scheme for the time-accurate incompressible Navier–Stokes equations. AIAA J 28(2):253–262
15. Shah A, Yuan L, Khan A (2010) Upwind compact finite difference scheme for time-accurate solution of the incompressible Navier–Stokes equations. Appl Math Comput 215(9):3201–3213
16. Gaitonde DV, Visbal MR (1999) Further development of a Navier–Stokes solution procedure based on higher-order formulas. Technical paper, 1999–0557. AIAA Press, Washington, DC
17. Visbal MR, Gaitonde DV (2002) On the use of higher-order finite-difference schemes on curvilinear and deforming meshes. J Comput Phys 181:155–185
18. Allen S, Cahn JW (1979) A microscopic theory for antiphase boundary motion and its application to antiphase domain coarsening. Acta Metall 27:1084–1095

19. Yana D, Ruo L, Tang T (2008) General moving mesh framework in 3D and its application for simulating the mixture of multi-phase flows. Commun Comput Phys 3(3):582–602
20. Zhang Z, Tang H (2007) An adaptive phase field method for the mixture of two incompressible fluids. Comput Fluids 36:1307–1318
21. Lele SK (1992) Compact finite difference schemes with spectral-like resolution. J Comput Phys 103:16–42
22. Zhang J, Qian Z (2012) Implicit eighth-order central compact scheme for the numerical simulation of steady and unsteady incompressible Navier–Stokes equations. Int J Comput Fluid Dyn 26:247–261
23. Carpenter MH, Gottlieb D, Abarbanel S (1993) The stability of numerical boundary treatments for compact high-order finite-difference schemes. J Comput Phys 108:272–295
24. Beam R, Warming RF (1978) An implicit scheme for the compressible Navier–Stokes equations. AIAA J 16:393–402
25. Pulliam T, Chaussee D (1981) A diagonal form of an implicit approximate-factorization algorithm. J Comput Phys 39:347–363
26. Yuan L (2002) Comparison of implicit multigrid schemes for three-dimensional incompressible flows. J Comput Phys 177:134–155
27. Zhijun T, Lim KM, Khoo BC (2007) An adaptive mesh redistribution method for the incompressible mixture flows using phase-field model. J Comput Phys 225:1137–1158
28. Kay D, Welford R (2006) A multigrid finite element solver for the Cahn–Hilliard equation. J Comput Phys 212:288–304
29. Bao K, Shi Y, Sun S, Wang XP (2012) A finite element for the numerical solution of the coupled Cahn–Hilliard and Navier–Stokes system for moving contact line problems. J Comput Phys 231:8083–8099